JOURNAL OF MATERIALS SCIENCE **39** (2004) 3605–3611

Determination of mechanical properties of pulsed laser-deposited hydroxyapatite thin film implanted at high energy with N^+ and Ar^+ ions, using nanoindentation

H. PELLETIER*, V. NELEA, P. MILLE
Laboratoire d'Ingénierie des Surfaces, Institut National des Sciences Appliquées, 24 Bld. de la Victoire, F-67084 Strasbourg, France
E-mail: pelletier@mail.insa-strasbourg.fr

D. MULLER
Laboratoire PHASE, CNRS, UPR 292, 23 rue de Loess, BP 20CR, F-67037 Strasbourg, France

Hydroxyapatite (HA) is extensively studied for various applications in bone implantology. We report here a comparison between the effects of ion beam implantation treatment using nitrogen and argon ions, on the mechanical characteristics of HA films grown by pulsed laser deposition. We used for deposition a KrF* excimer laser. Crystalline and stoichiometric HA films were grown on Ti-5Al-2.5Fe alloy substrate, previously coated with a TiN buffer layer. After deposition, the film were implanted with ions of N^+ and Ar^+ of high energy (1–1.5 MeV range) and dose set at 10^{16} at cm^{-2}. The hardness and elastic modulus were determined by nanoindentation tests using a spherical tipped nanoindenter with a 5 μm-tip radius. From the load-displacement curves, we put into evidence an enhancement of the mechanical characteristics of the HA films after implantation, especially for those implanted with N^+ ions. This improvement of the mechanical characteristics is related to the changes of surface morphology and the densification of the HA layer after ion treatment.

1. Introduction

Hydroxyapatite (HA) is extensively studied for various applications in bone implantology. Applied as coatings and thin films, HA increases the biocompatibility of the titanium-based prostheses, showing excellent bioactivity and osteoconductivity [1]. However, the mechanical properties (hardness and elastic modulus) of these structures are generally poor. These low characteristics are related to the poor intrinsic mechanical characteristics of the HA material, but also to the lack in density of the produced films [2, 3]. High energy ion-beam implantation was proved to be an appropriate tool for surface modification and densification of materials [4]. Therefore, the mechanical resistance of the HA films can be increased by ion bombardment. However, the main hardening mechanism after ion implantation is not well established.

We report here a comparison between the effects of ion beam implantation treatment using nitrogen and argon ions, on the mechanical characteristics of HA films grown by pulsed laser deposition. Compared to the previous studies [2–4], to evaluate mechanical properties, we have used depth sensing indentation test with a spherical tipped indenter.

2. Experimental procedure

The HA thin films were grown in a stainless steel deposition chamber evacuated down to 10^{-4} Pa residual pressure. We used a KrF* excimer laser ($\lambda = 248$ nm, $\tau_{FWHM} \geq 20$ ns) delivering pulses of 80 mJ energy. Using a MgF_2 cylindrical lens the laser beam was focused at 45 degree on a hot-pressing pellet made from high-purity (99.98%) polycrystalline HA powder (<100 μm particles size). More details of the used pulsed laser deposition installation can be found in Ref. [5]. We used as substrates disks (1 mm thickness) cut from Ti-5Al-2.5Fe (TiAlFe) alloy bar (20 mm diameter). The substrates were gradually mechanical polished with SiC abrasive papers (ultimate grit 1000) and subsequently using diamond suspension solution (<0.25 μm size grains). The temperature of the substrate was measured by a very thin thermocouple glued also with argent paste on the substrate surface. The substrates were placed parallel to the HA target at a distance of 4 cm. Before HA films deposition, the TiAlFe substrate was coated with a ceramic TiN buffer layer. The laser fluence was set at 1 Jcm^{-2}. A series of 10^4 subsequent laser pulses were applied for a HA single film growth. The substrates were kept at room temperature during HA depositions

*Author to whom all correspondence should be addressed.

and the as-deposited films were subsequently annealed in air at 550°C for 1 h with both heating and cooling rate of 2°C/min. The buffer layers were created also by PLD by ablating stoichiometric TiN targets. The TiN layers were grown in low-pressure nitrogen atmosphere (10^{-1} Pa) on substrate heated at 650°C temperature. The deposited HA films had a thickness of $\sim$1 μm, while the thickness of the TiN buffer layers varied between 200 and 500 nm.

Using a Van de Graaff-type implanter [6], the samples were then implanted at a constant dose of 10^{16} cm^{-2} (keeping the current density at 1 μAcm^{-2}) with energies of 1 and 1.5 MeV, respectively for nitrogen (sample S1) and argon (sample S2). The sample temperature was maintained below room temperature, with liquid nitrogen cooling to prevent heating effects and to avoid implanted atoms redistribution during implantation treatment.

Before performing ion implantation and in order to choose the adapted energy to the different composites, Ar^+ and N^+ distribution simulations were performed using TRIM® code [7]. The theoretical projection can be described by the projected range (R_P), by its standard deviation (ΔR_P) and by the maximal concentration (C_{max}) of the implanted atoms.

Fig. 1 shows typical theoretical distributions as a function of ion energy for the specific composites HA/TiN/Ti, where the buffer layer thickness of both composite systems is supposed to be about 500 nm.

The hardness (H) and elastic modulus (E) were determined using a commercially available ultralow load indentation system, the NANO INDENTER® XP (MTS, Nano Innovation Center, Oak Ridge, TN), equipped with a spherical tipped indenter having the tip radius (R) of 5 μm. This highly sensitive mechanical properties microprobe has the capability of sensing both load (P) and displacement (h) continuously as indents are being made in a sample, with resolutions of up to 75 nN and 0.04 nm, respectively. Multiple indentations were made at different peak loads (P_{max}) of 1, 10, 50 and 100 mN on different HA film surfaces of each sample: unimplanted and implanted zones. At each peak load, the (P)-(h) curve was recorded from which E and H are calculated using standard equations, deduced from the Oliver-Pharr model [8]. During the loading phase to the peak load value, we have programmed several partial

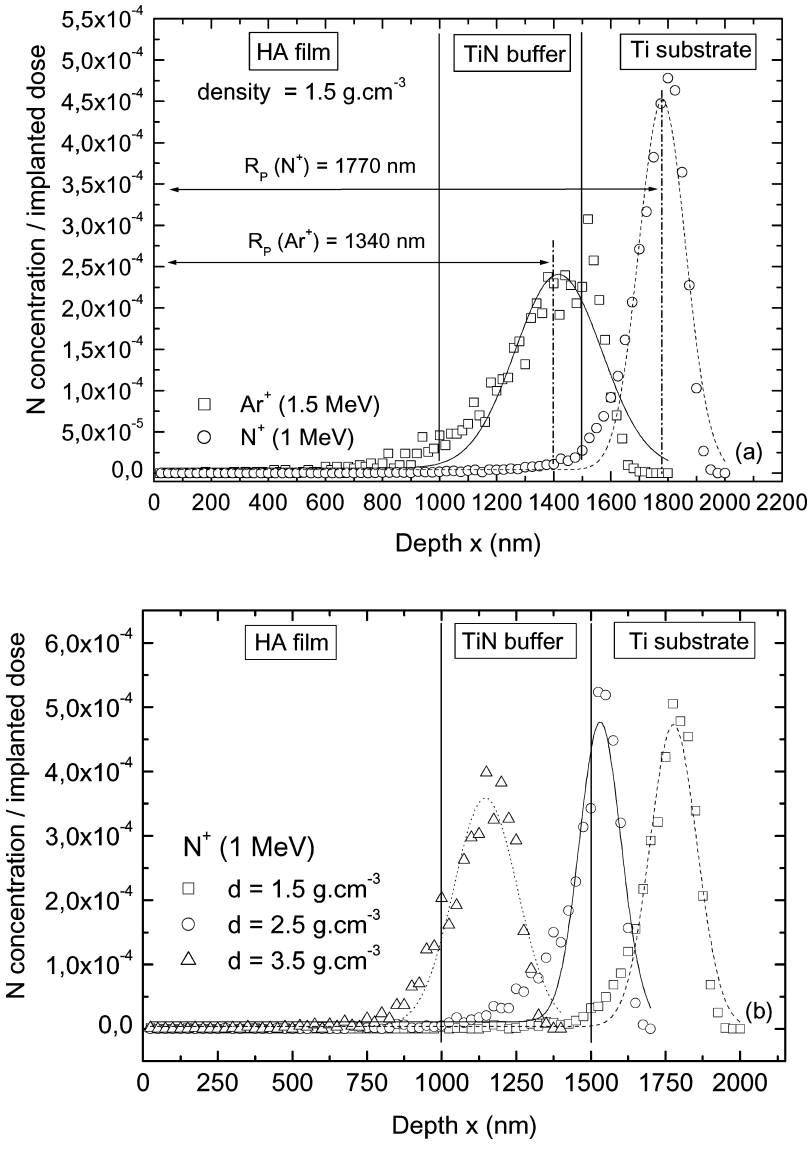

Figure 1 Ar^+ and N^+ distributions simulated with TRIM code (a) and evolution of N^+ distribution as a function of HA film densisty (b).

unloading phases, to get hardness and elastic modulus at lower applied loads, and then to follow with more accuracy the evolution of elastic and plastic mechanical properties through the HA film thickness. For each studied area, the H and E values at a given applied load represent the average of at least five indents and their associated scatter bars are the corresponding standard deviations.

Compared to trigonal indenter (sharp Berkovich tip), an attractive feature of a spherical tipped indenter is that the initial response of a material is elastic and then at a critical load, the onset of plasticity occurs. But, the absence of geometrical similarity enables a changing contact strain to be reflected in a changing contact pressure [9]. This kind of tip geometry appears to be not well adapted for materials having a gradient of mechanical properties, such as multi-layer systems. We try here to classify the different zones using comparative results from the same experimental test. The interpretation of the load-displacement behavior of a spherical tipped indenter is more complex that those obtained with a Berkovich indenter.

Swain and Field [10] derived a procedure for deconvoluting elastic-plastic load-displacement data. First, they suppose that the contact indentation depth, h_C, is lying mid way between the maximum depth of penetration, h_T, (measured at P_{max}) and the residual impression depth, h_R. But, in our opinion, the contact depth depends on the elastic-plastic behavior of the indented material. Thus, we use the same formula than Oliver and Pharr method [11] to determine h_C from the unloading phase of the experimental (P)-(h) curve:

$$h_C = h_T - \frac{P_{max}}{S} \tag{1}$$

with (S), stiffness calculated from the slope of the unloading phase $S = \frac{dP}{dh}|_{h=h_T}$. We estimate the contact radius with the following equation with $R = 5\ \mu$m:

$$a_C = \sqrt{2Rh_C - h_C^2} \tag{2}$$

Indentation data may be therefore represented as a plot of mean pressure (p_m) versus the a/R ratio which has the form of a stress-strain curve:

$$p_m = \frac{P}{\pi a_C^2} \tag{3}$$

$$\varepsilon = 0.2\frac{a_C}{R} \tag{4}$$

3. Results and discussion

We used ion implantation treatment at high energy to create through the HA layer thickness a gradient of defects, first at the crystalline lattice level, and also at the microscopic scale. These defects are due to the nuclear collisions between the incident particles (N^+ and Ar^+) and the different target atoms, which compose the HA layer and the buffer TiN layer. Another effect of ion implantation into such multi-layer systems is related to the introduction of compressive residual stress into the layer. But, here, the implanted dose is clearly not sufficient for create important level of residual stress. Moreover, with adapted incident particles (to be defined), we may think that a chemical effect is also expected in future. To get a good biocompatibility for biomedical applications, the HA layers have to be crystalline with a proper Ca/P ratio. In the previous article [4], we have verified with grazing incidence X-ray diffraction that the implantation process at high energy does not modify the stochiometric composition of the HA layer surface. The implantation energy for the two implanted species have been determined with TRIM simulation, to obtain a projected ion range greater than the average HA layer thickness ($R_p \geq 1\ \mu$m). The aim is to avoid chemical effects in the HA layer and then to create defects around the interface between the HA layer and the underlying TiN layer. But the real density of the PLD HA layer is an unknown parameter for TRIM simulation. It can varies between 1.5 to 3.15 g cm^{-3}.

Fig. 1b shows for N^+ implantation at 1 MeV the evolution of the nitrogen concentration distribution as a function of the HA layer density. The projected ion range varys from 1.77 to 1.15 μm, and from 1.34 to 0.80 μm, for implantation with nitrogen and argon, respectively. Assuming an average density of HA film of about 2.5 g cm^{-3}, the maximum concentration of implanted element is located within the TiN layer.

Fig. 2 shows the evolution of mechanical properties of films after nitrogen implantation. We have

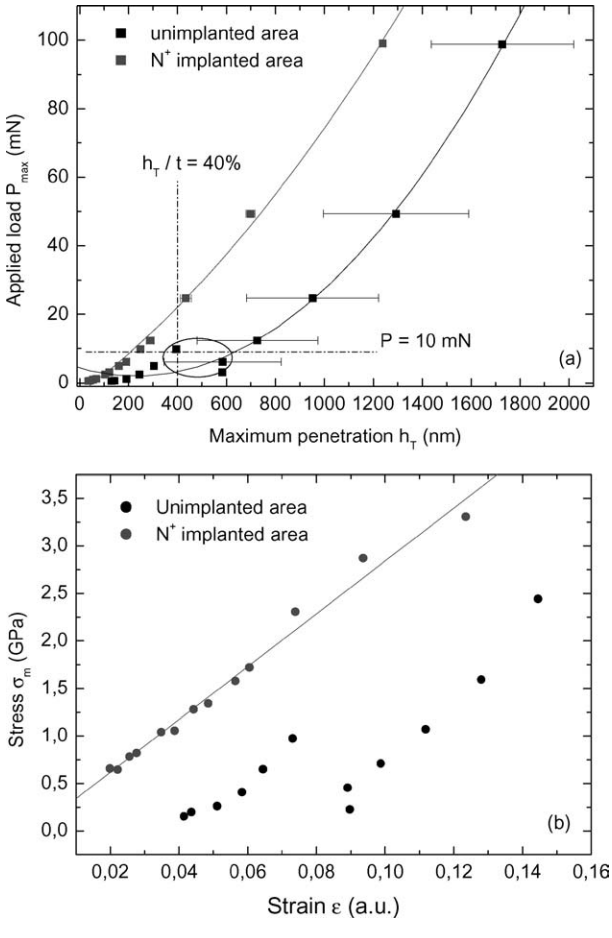

Figure 2 Evolution of mechanical properties measured by nanoindentation for sample S1 implanted with nitrogen (1 MeV): (a) resistance to penetration and (b) stress-strain curve p_m vs. ε as a function of the indented zone.

represented the curves of resistance to penetration, applied load vs. indentation depth, (Fig. 2a) obtained in normal static test at low strain rate. Although this curve is directly related to the indenter geometry, this qualitative information shows the benefit of nitrogen implantation. We observe a strong difference between the unimplanted and implanted zones. This difference appears for low indentation depth (about 200 nm) while the thickness layer affected by the ion bombardment is located deeper. This phenomenon is often noted for the characterization of thin films on substrate or implanted surfaces using nanoindentation [12, 13]. During indenter penetration into a surface, an elastic and plastic cavity (influence zone) is formed, whose radius increase with indentation depth. For spherical tipped indenter, the average value of strain in the cavity depends on the ration a/R (Equation 4). This particular strain field beneath the spherical tip explains the rapid evolution of the resistance to penetration of N^+ implanted zone. The resistance to penetration curve of the unimplanted zone presents a large step for indentation depth around 400 nm, corresponding to an average ratio $h_T/t = 40\%$ (with t = HA layer thickness). For h_T = 400 nm the influence zone beneath the indenter tip reaches the HA/TiN interface [14]. This step is, according to us, correlated with a delamination phenomenon of the HA layer. However, optical micrographs do not show any fracture around the residual imprint, performed at high load. Other load-displacement curves obtained in the unimplanted zone (Fig. 3) exhibit many steps or pop-ins during the loading phase. According to Hainsworth *et al*. [15], these pop-ins can be also related to formation and the propagation of cracks into the HA film. We think that these steps are caused by cracks through the film thickness because of film porosity, as observed by TEM [5]. Moreover, the growth of the PLD films produces a mixed structure, with columnar parts and droplets, which can explain this behavior of the unimplanted HA layer during tip penetration. No steps or pop- ins are detected after nitrogen implantation.

This feature proves that the implantation process produce some important changes in the HA film, especially around the HA/TiN interface, both due to the increase of defect density and to the ion beam mixing in the near interface region.

Fig. 2b represents the evolution of the mean contact pressure p_m (Equation 3) as a function of the average strain (Equation 4). In the nitrogen implanted zone, the p_m values increases with strain, and this evolution between 0.7 GPa ($\varepsilon = 2\%$) and 3.30 GPa ($\varepsilon = 12\%$) can be approximated by a linear function. In Table I, we

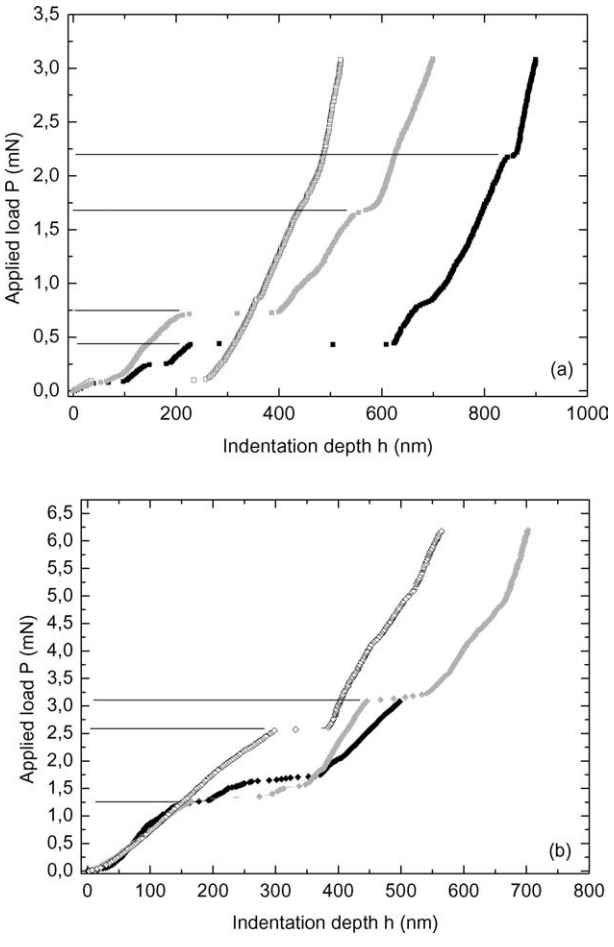

Figure 3 Examples of load-displacement curves obtained in the unimplanted zone (sample S1). We have plotted only the loading part of the curves.

have summarized the nanoindentation results for each samples S1 and S2, in the unimplanted and implanted zones. The values of mean contact pressure and elastic modulus are determined at specific applied load, about 0.5 and 3 mN, for unimplanted and implanted zones, respectively, because these loads correspond to an average ratio indentation depth, h_T, on HA film thickness, t, of about 10%. In this range of indentation depth, we may assume that the measured mechanical properties are not affected by the underlying layers (TiN and Ti substrate), and can be considered as intrinsic characteristics of HA films [14]. An important improvement of mechanical properties can be noted after implantation with nitrogen, with an increase of hardness with a factor 5, and of elastic modulus with a factor 2.65. On the p_m vs. ε curve of the unimplanted zone, a

TABLE I Evolution of mechanical properties measured by nanoindentation as a function of analysed area, corresponding to a ratio $h_T/t = 10\%$

Sample	Analysed area	Applied load P_{max} (mN)	Indentation depth h_T (nm)	Contact stress p_m (GPa)	Elastic modulus E (GPa)
S1	Unimplanted	0.5	129 (±51)	0.15 (±0.05)	15 (±11)
S2	Unimplanted	0.5	136 (±115)	0.20 (±0.12)	20 (±10)
S1	Implanted N^+ (zone 1)	3	119 (±12)	1.12 (±0.16)	56 (±7)
S1	Implanted N^+ (zone 2)	3	128 (±10)	1.00 (±0.10)	53 (±5)
S2	Implanted Ar^+ (zone 1)	3	156 (±51)	0.84 (±0.15)	54 (±6)
S2	Implanted Ar^+ (zone 2)	3	285 (±35)	0.39 (±0.13)	43 (±6)

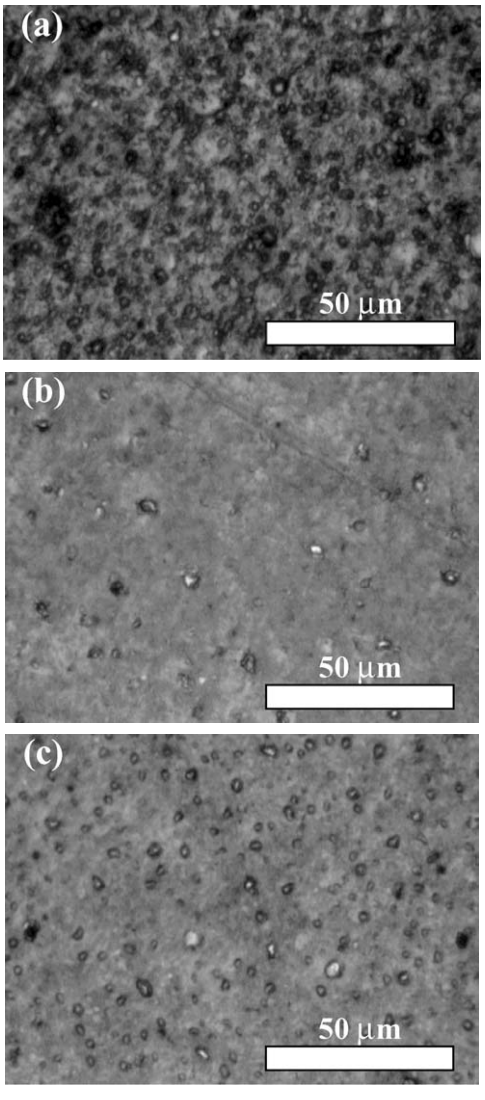

Figure 4 Optical micrograph of the different tested zones after N^+ implantation: (a) unimplanted, (b) as implanted zone 1, and (c) as implanted zone 2.

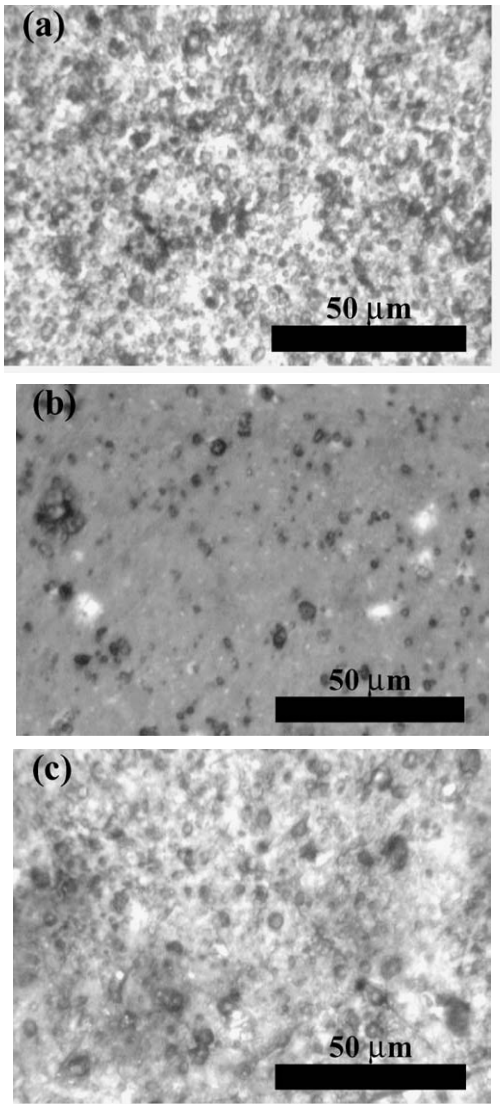

Figure 5 Optical micrograph of the different tested zones after Ar^+ implantation: (a) unimplanted, (b) as implanted zone 1, and (c) as implanted zone 2.

break, correlated with the pop-ins previously described in Fig. 3, is determined for an strain average value of about 8%. This value is very interesting because it corresponds to the average strain in the influence zone generated by a Berkovich indenter. This remark may explain the lack of sensibility with nanoindentation test using a trigonal indenter, observed in the previous studies [2–4].

We observe in Table I the good reproductibility both in the unimplanted zones (samples S1 and S2) and in the N^+ implanted zones, noted 1 and 2. The implanted zones 1 and 2 are defined in Fig. 4. The optical micrographs show the surface morphology of HA film before and after nitrogen implantation. Different zones in the implanted area can be distinguished. We can compare the evolution of topography of the surface after implantation, more or less in good correlation with roughness measurements in Table I. In the treated area, we observe a progressive decrease of the surface density and the size of droplets (Fig. 4b and c). In the two implanted zones (1) and (2), we have realized a series of 9 indentations at peak load $P = 5$ mN. In the case of nitrogen implantation, we note a small scattering in experimental measured properties between the two implanted zones. These results evidence that there is no direct relationship between the density or size of droplets and the mechanical properties estimated with nanoindentation test.

Fig. 5b and c show that implantation with argon generates on the HA film surface a variation of morphology, by comparison with the unimplanted area (Fig. 5a). The surface morphology obtained in the Ar^+ implanted zone, noted (1) in Fig. 5b, is similar to the one observed after nitrogen implanation, with some visible droplets dispersed in a homogeneous matrix. However, as proved by Fig. 5c, some areas look like the unimplanted zone. We have performed in the different zones, a high number of indentations, with at least 9 indentations per applied peak load in the range of 1 to 100 mN. The obtained results are regrouped both in Table I and in Fig. 6. We have plotted the resistance to penetration curves (Fig. 6a), the evolution of mean contact pressure (Fig. 6b) and of elastic modulus (Fig. 6c), as a function of indented zones. Compared to nitrogen implantation, we observe here a strong dependancy of measured mechanical properties with surface morphology. The best

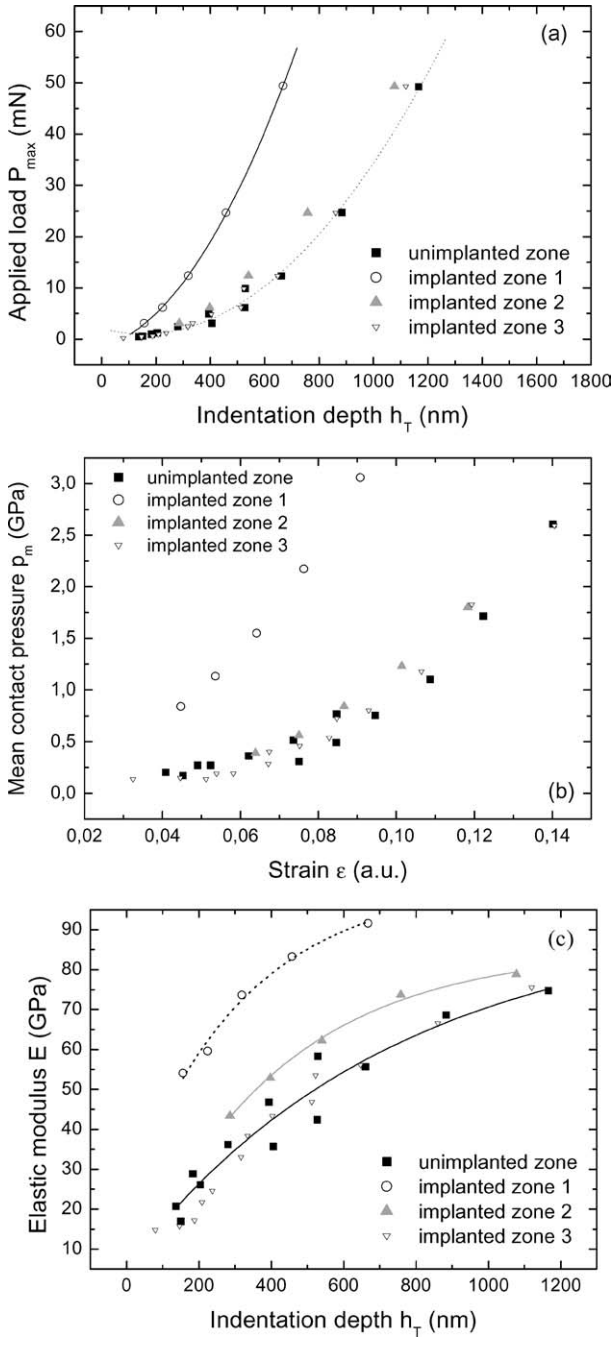

Figure 6 Evolution of mechanical properties measured by nanoindentation for sample S2 implanted with argon (1.5 MeV): (a) resistance to penetration, (b) stress-strain curve p_m vs. ε, and (c) elastic modulus vs. indentation depth, as a function of the indented zone.

results are obtained for the zone 1 (Fig. 5b), and are similar to those calculated after nitrogen implantation (Table I). But, in the zones 2 and 3, the measured values are low. The curves, shown in Fig. 6, corresponding to the implanted zones 2 and 3, are similar to the data measured for unimplanted zone. We note a small improvement of mean contact pressure and elastic modulus, especially for the zone 2. But, the values of p_m and E reported in Table I are estimated at $h_T = 285$ nm, corresponding to a ratio h_T/t near 30%. For this range of indentation depth, the measured mechanical properties (especially the elastic modulus) can be influenced by the mechanical properties of the underlying TiN layer. Moreover, the mean contact pressure of the zone 2 implanted with argon is deduced for an average strain value of about 7%, although the other contact stress values regrouped in Table I have been determined for strain less than 5%.

Compared to the nitrogen implantation, the HA film implanted with argon is not homogeneous and the mechanical properties are dependant on the morphology of the layer. This correlation is not well understood, but we may assume that it seems to be related with the size of the incident particule. To explain both the variation of morphology after implantation at high energy and of mechanical properties, the next step consists in the determination of the hardening mechanisms as a function of the ion species. However, if we consider only the zone 1 both for nitrogen (Fig. 2b) and argon (Fig. 6b) implantation, we conclude that the implantation process results in an important improvement of mechanical properties, which seems to be independant of the implanted ion. Indeed, for bulk metallic materials, the curves showing the mean contact pressure vs. average strain can be easily related to the constitutive law obtained with a classical tensile test [9, 10]. This curve provides direct information about the intrinsic mechanical properties of the multilayer system. The p_m vs. ε curves are not influenced by the tip geometry used to performe the indentation tests. The variation of the constitutive law of the HA layer and of the multilayer system after implantation with nitrogen or argon demonstrates that the implantation process (after an optimisation of the implantation parameters) can yield to an important increase of the lifetime of mechanical articulating parts of an orthopedic prosthesis, coated with a PLD HA layer. We suppose that the implantation treatment is an interesting tool to improve the abrasive wear resistance of PLD films.

4. Conclusion

We have investigated the ability of ion implantation at high energy into pulsed laser deposition of hydroxyapatite films. The implantation process with nitrogen and argon does not modify in the surface region the HA crystalline structure, produced by laser deposition and improve the mechanical resistance of HA layer. After implantation, we have demonstrated an increase of hardness and elastic modulus of the HA layer, respectively with a factor of 5 and of 2.65 with a good reproductibility for nitrogen implantation. These variations may yield to an important improvement of wear resistance, and then to the increase of the applications of such coatings, especially for biomedical devices.

However, new analysis (TEM, RBS, GIXRD) are in progress to identify the hardening mechanism produced by ion implantation treatment into such multilayer systems. Other implantations with different fluences, energies and treatment temperatures are also programmed, to find the best implantation parameters, and then optimize the process.

References

1. H. ZENG, W. R. LACEFIELD and S. MIROV, *J. Biomed. Mater. Res.* **50** (2000) 248.

2. V. NELEA, C. RISOTU, C. CHIRITESCU, C. CHICA, I. N. MIHAILESCU, H. PELLETIER, P. MILLE and A. CORNET, *Appl. Surf. Sci.* **168** (2000) 127.
3. V. NELEA, H. PELLETIER, I. ILIESCU, J. WERCKMANN, V. CRACIUN, I. N. MIHAILESCU, C. RISOTU and C. CHICA, *J. Mater. Sci.: Mater. Med.* **13** (2002) 1167.
4. V. NELEA, H. PELLETIER, D. MULLER, N. BROLL, P. MILLE, C. RISTOSCU and I. N. MIHAILESCU, *Appl. Surf. Sci.* **186** (2002) 483.
5. V. NELEA, Ph.D. thesis, University of Strasbourg (ULP), France, 2002.
6. J. P. STOQUERT, J. J. GROB and D. MULLER, *Nucl. Inst. Meth.* B **79** (1993) 664.
7. U. LITTMARK and J. F. ZIEGLER, *Phys. Rev.* **23A** (1981) 64.
8. W. C. OLIVER and G. M. PHARR, *J. Mater. Res.* **7**(6) (1992) 1564.
9. D. TABOR, "Hardness of Metals" (Clarendon Press, Oxford, 1951).
10. M. V. SWAIN, *Mater. Sci. Engng.* A **253** (1998) 160.
11. E. G. HERBETT, G. M. PHARR, W. C. OLIVER, B. N. LUCAS and J. L. HAY, *Thin Solid Films* **398/399** (2001) 331.
12. H. PELLETIER, P. MILLE, A. CORNET, J. J. GROB, J. P. STOQUERT and D. MULLER, *Nucl. Instr. Meth. Phys. Res.* B **148** (1999) 824.
13. *Idem.*, *ibid.* B **178**(1–4) (2001) 319.
14. N. G. CHECHENIN, J. BOTTINGER and J. P. KROG, *Thin Solid Films* **261** (1995) 219.
15. T. F. PAGE and S. V. HAINSWORTH, *Surf. Coat. Techn.* **61** (1993) 201.

Received 29 July 2003
and accepted 8 March 2004